

Calcium Dynamics in Root Cells of *Arabidopsis thaliana* Visualized with Selective Plane Illumination Microscopy

Alex Costa^{1*}, Alessia Candeo², Luca Fieramonti², Gianluca Valentini², Andrea Bassi²

¹ Dipartimento di Bioscienze, Università degli studi di Milano, Milano, Italy, ² Dipartimento di Fisica, Politecnico di Milano, Milano, Italy

Abstract

Selective Plane Illumination Microscopy (SPIM) is an imaging technique particularly suited for long term *in-vivo* analysis of transparent specimens, able to visualize small organs or entire organisms, at cellular and eventually even subcellular resolution. Here we report the application of SPIM in Calcium imaging based on Förster Resonance Energy Transfer (FRET). Transgenic *Arabidopsis* plants expressing the genetically encoded-FRET-based Ca²⁺ probe Cameleon, in the cytosol or nucleus, were used to demonstrate that SPIM enables ratiometric fluorescence imaging at high spatial and temporal resolution, both at tissue and single cell level. The SPIM-FRET technique enabled us to follow nuclear and cytosolic Ca²⁺ dynamics in *Arabidopsis* root tip cells, deep inside the organ, in response to different stimuli. A relevant physiological phenomenon, namely Ca²⁺ signal percolation, predicted in previous studies, has been directly visualized.

Citation: Costa A, Candeo A, Fieramonti L, Valentini G, Bassi A (2013) Calcium Dynamics in Root Cells of *Arabidopsis thaliana* Visualized with Selective Plane Illumination Microscopy. PLoS ONE 8(10): e75646. doi:10.1371/journal.pone.0075646

Editor: Malcolm Bennett, University of Nottingham, United Kingdom

Received: February 22, 2013; **Accepted:** August 19, 2013; **Published:** October 16, 2013

Copyright: © 2013 Costa et al. This is an open-access article distributed under the terms of the Creative Commons Attribution License, which permits unrestricted use, distribution, and reproduction in any medium, provided the original author and source are credited.

Funding: This work was partially supported by Futuro in Ricerca 2010 RBF1051LJ_001 grant. The funders had no role in study design, data collection and analysis, decision to publish, or preparation of the manuscript. No additional external funding were received for this study.

Competing Interests: The authors have declared that no competing interests exist.

* E-mail: alex.costa@unimi.it

Introduction

Calcium (Ca²⁺) is a multifaceted second messenger in eukaryotic organisms. In plants, Ca²⁺ is involved in many aspects of development and takes part into different regulatory processes [1,2]. Plant cells respond to several environmental or developmental stimuli, by changing the intracellular free Ca²⁺ concentration. These changes are commonly referred as “Ca²⁺ signatures” and can range from a single transient increase to a series of repetitive Ca²⁺ oscillations [3–7]. The leading hypothesis states that different Ca²⁺ signatures might encode specific information, leading to distinct downstream responses [3–9]. Several examples in support of such hypothesis have been reported in single cell systems, such as guard cells [3,4] and root hairs of leguminous species [10] but also in entire seedlings. In the latter case, imposing distinct Ca²⁺ elevations differentially affected gene expression [11,12]. The introduction of genetically encoded Ca²⁺ indicators (e.g. aequorin and GFP-based Ca²⁺ probes), has permitted the detection and visualization of intracellular Ca²⁺ dynamics in living plants [13,14]. Experiments performed using aequorin produced reliable data, but could only show the response of a population of cells or plants, not allowing the investigation of intercellular heterogeneities. In order to improve cellular and subcellular resolution, the use of other Ca²⁺ sensors has been pursued in recent years and, among the genetically encoded Ca²⁺ indicators, Cameleons are the most frequently used [14–20]. Cameleons are Förster Resonance Energy Transfer (FRET) based indicators in which two fluorescent proteins, CFP and YFP (or circularly permuted variants of YFP), are linked together by the calcium-binding protein calmodulin and a calmodulin binding peptide. Binding of Ca²⁺ to these calcium-responsive elements alters the distance between the two fluorophores hence the efficiency of

FRET, allowing a quantitative measurement of Ca²⁺ dynamics [21]. In particular, one of the most employed FRET probes in plant biology is the Yellow Cameleon YC3.6 [22], which has been specifically designed to improve the brightness and energy transfer between the FRET couple, CFP and cpVenus. The YC3.6 probe has several peculiar properties that fit well the needs of plant biology: i) high signal to noise ratio; ii) high dynamic range; iii) pH stability in the physiological range; iv) an *in vitro* K_d for Ca²⁺ of 250 nM [22]. All these features make Cameleon YC3.6 suitable

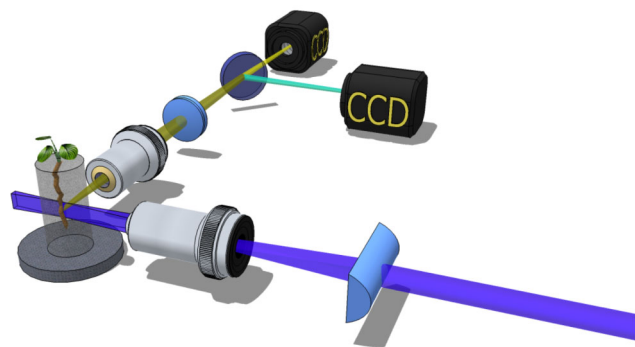


Figure 1. Schematic of the SPIM-FRET setup: a cylindrical lens in combination with a microscope objective create a light-sheet on the sample orthogonal to the detection axis. Two CCDs are used to image the CFP (Fluorescence) and cpVenus (FRET) signals. Note that for the simultaneous acquisition of the two channels, several configurations are possible: i) two independent cameras; ii) a camera with two CCDs; iii) a single camera coupled with a beam splitter can be used (not shown in the cartoon).

doi:10.1371/journal.pone.0075646.g001

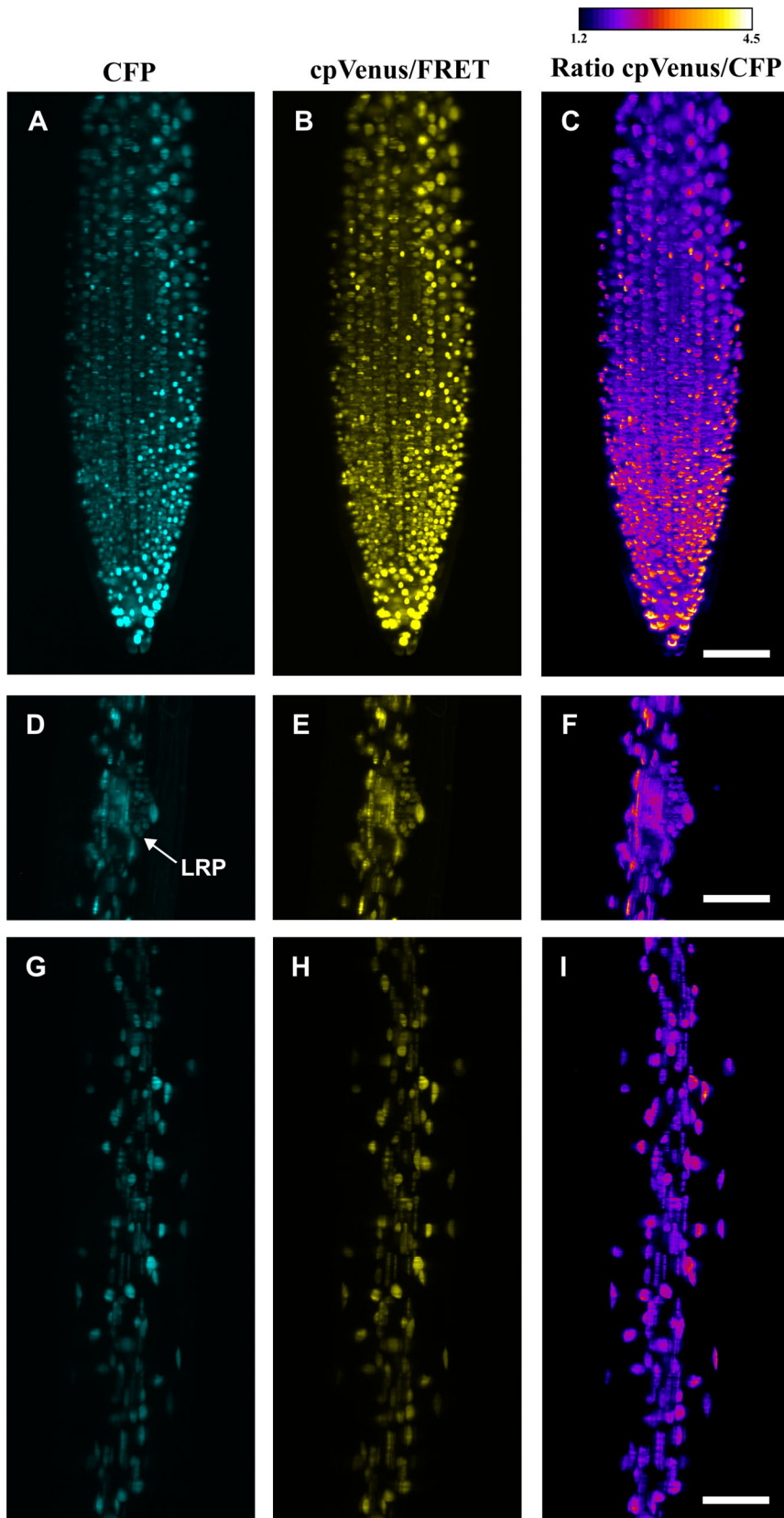


Figure 2. Maximum intensity projections of the stacks obtained for CFP (A,D,G), cpVenus/FRET (B,E,H) and Ratio between the two channels (C,F,I) in different regions of the *Arabidopsis thaliana* root (primary root tip, lateral root primordium and root mature zone) expressing the nuclear localized Cameleon. LRP: lateral root primordium. Scale bar is 50 μ m.
doi:10.1371/journal.pone.0075646.g002

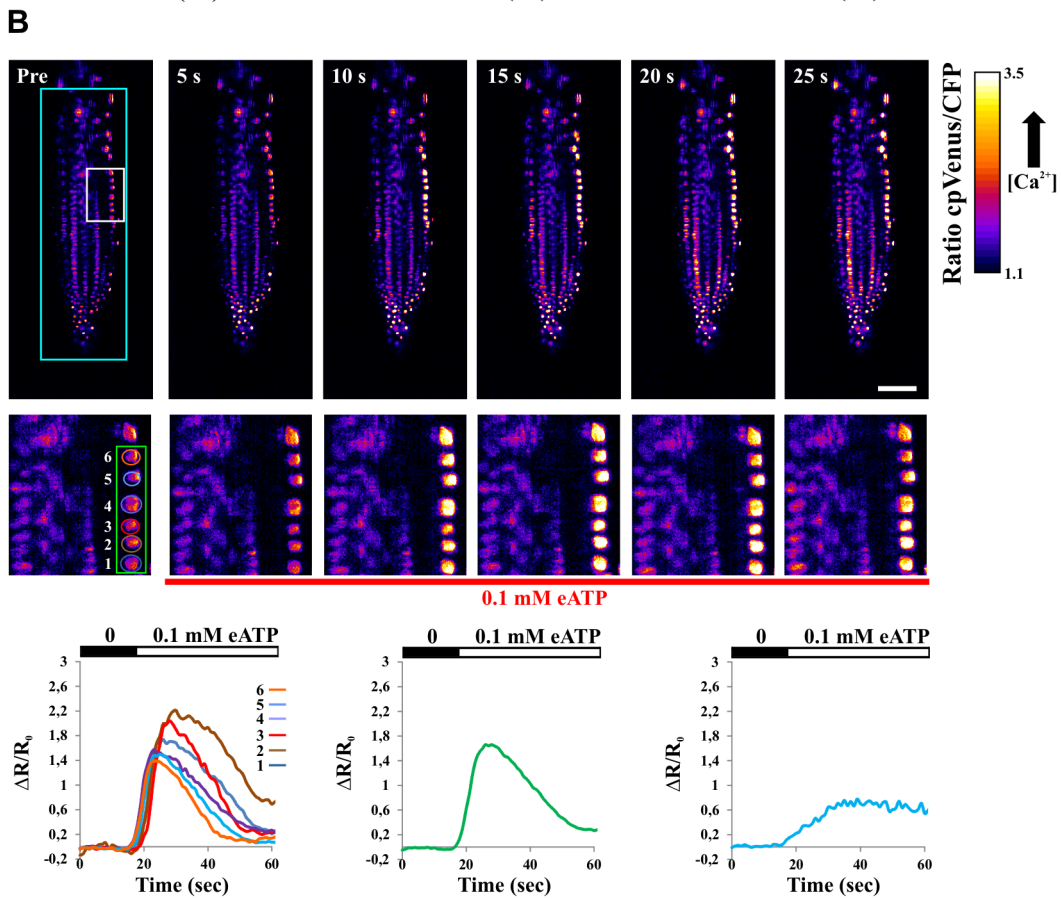
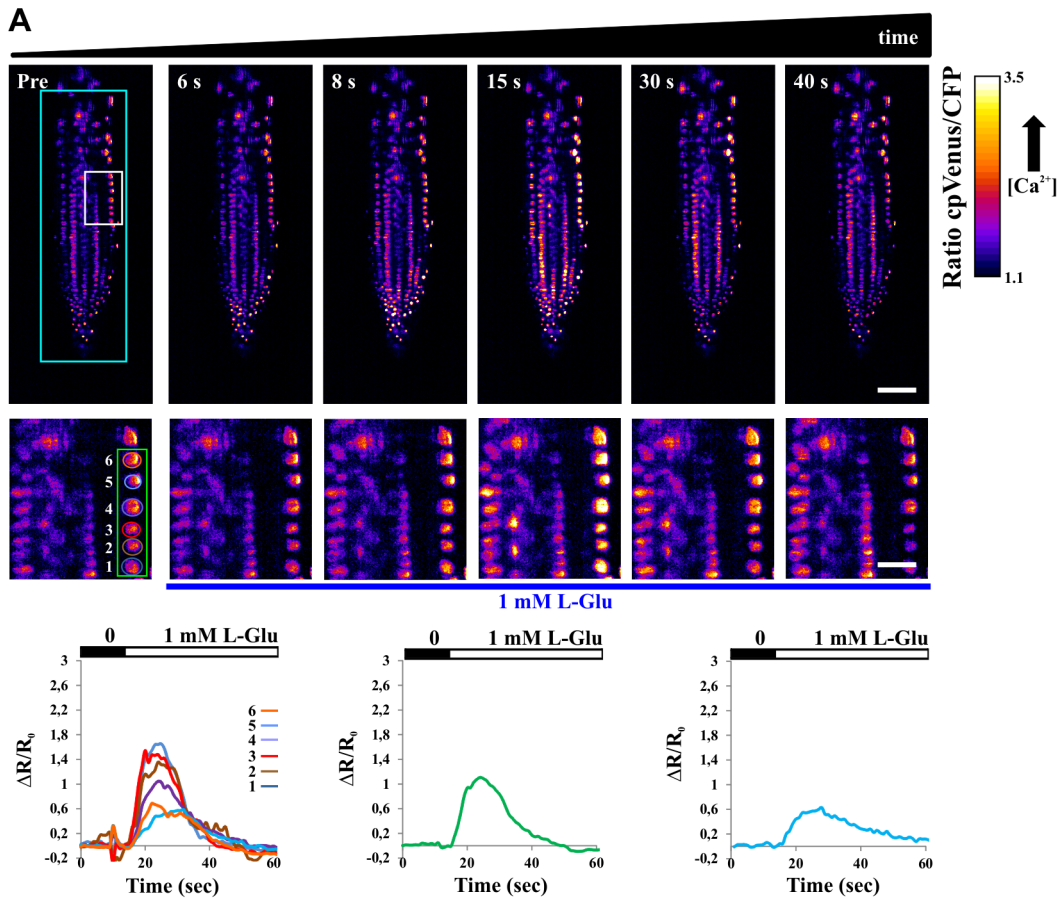


Figure 3. Single plane FRET ratio in root tip of Arabidopsis seedlings expressing the nuclear localized Cameleon, measured at different times in the course of 1 mM L-Glu (A) and 0.1 mM eATP (B) stimuli. (A) First row: FRET ratio images at different time points from the sensing (Pre) of the L-Glu stimulus. Second row: close up (white rectangle in the top-left image) of the FRET ratios including 6 selected nuclei (green rectangle). Third row: temporal evolution of the FRET ratio in the 6 distinct nuclei (left), average on the 6 nuclei (center), average on the entire plane (right). (B) First row: FRET ratio images at different time points from the sensing (Pre) of the eATP stimulus. Second row: close up (white rectangle in the top-left image) of the FRET ratios including 6 selected nuclei (green rectangle as in panel A). Third row: temporal evolution of the FRET ratio in the 6 distinct nuclei (left), average on the 6 nuclei (center), average on the entire plane (right). Scale bar is 50 μm and 10 μm for low and high magnifications respectively.
doi:10.1371/journal.pone.0075646.g003

for Ca^{2+} sensing in different cell types and possibly in subcellular compartments [19,20,23].

The *in-vivo* visualization of FRET sensors in complex plant organs/tissues such as the root, is possible with standard microscopy modalities, all of which present different limitations.

Wide-field microscopy has been successfully used with the main limitation of absence of depth sectioning [19,20], the Ca^{2+} response is averaged over the entire volume, analysis at single cell resolution is not possible and, as a result, only the averaged cellular response can be observed. Single cell resolution in the root has been achieved by means of confocal laser scanning microscopy (CLSM) using Cameleon probes in response to both biotic and abiotic stimuli [16,17,19,24]. However, CLSM can cause strong photo-bleaching (in particular for repetitive three-dimensional measurements), the acquisition is slow or limited to a small volume, restricting the analysis to single or few cell layers [17,19,24,25]. Furthermore, in the majority of microscopes the plant is mounted horizontally on a glass slide. Although largely used, such specimen preparation can itself induce stress conditions or physiological responses such as hormone/s redistribution. A simple case occurs in the root tissues, where the auxin distribution is known to be regulated in response to a gravitropic stimulus [26].

In order to overcome these limitations, we used Selective Plane Illumination Microscopy (SPIM) to image Arabidopsis transgenic plants expressing the nuclear and cytosolic-targeted Cameleon YC3.6, previously generated by Schumacher and coworkers [19]. The system is equipped with parallel detection of two wavelength channels for ratiometric FRET imaging (Figure 1). SPIM [27] is a fluorescence microscopy technique, in which the illumination axis is perpendicular to the detection axis. A laser beam is used to create a thin light-sheet right in the focal plane of the detection objective. The light-sheet can be a few microns thin thus avoiding out of focus fluorescence and providing optical sectioning. The lateral resolution is given by the detection objective, yielding subcellular details. SPIM is well suited for rapid 3D *in-vivo* imaging of *Arabidopsis thaliana* specimens at high spatial resolution, with minimal photo-damage to the sample [28,29]. In fact, only the plane of the specimen under observation is illuminated. This configuration greatly reduces the light dose and therefore photo-bleaching and photo-toxicity. Another advantage of SPIM is that, during the entire analyses, the seedlings are placed in conditions similar to those used for their growth, with the root floating and growing in the water based solution and the shoot in free air (Figure 1).

Materials and Methods

SPIM apparatus

The microscope is a modified version of the OpenSPIM project [30], and it is similar to a single illumination arm SPIM [31]. A single mode fiber coupled laser at 442 nm (MDL-III-442, CNI) is collimated and used for SPIM illumination. An automatic shutter switches the beam on and off via computer control. A cylindrical lens focuses the light in a horizontal plane and a 1 \times telescope

images the focal plane of the cylindrical lens in the back focal plane of the illumination 10 \times water dipping microscope objective (UMPLFLN 10XW, Olympus). As a result, a vertical light-sheet is created on the sample in the front focal plane of this objective. A slit placed in the center of the telescope confines the excitation light-sheet within the imaged area. The height of the light-sheet is 600 μm and its thickness is about 3 μm (beam waist in the focal plane of the illumination objective). Typical illumination power at the sample was between 10 and 50 μW . We didn't observe any photo-bleaching (during continuous illumination for more than 5 minutes) for illumination powers below 15 μW . The detection unit consists in a 20 \times water dipping microscope objective (UMPLFLN 20XW, Olympus), a tube lens (U-TLU-1-2, Olympus), and a dual sensor CCD camera (Orca D2, Hamamatsu Photonics K.K.). The illumination and the detection microscope objectives are precisely aligned at 90 $^\circ$ in the imaging chamber, which is filled with a water-based solution. The detector consists of a dual-CCD system in which the two sensors are positioned at 90 $^\circ$ after a dichroic filter (at 510 nm). One of the two sensors can be rotated and translated to correct focus and alignment in order to produce high contrast images. In addition to the dichroic filter, two band-pass filters (centered at 483 and 542 nm) are used to detect CFP and cpVenus (FRET) signals simultaneously. A white-LED illuminator in transmitted light configuration is used during the alignment of the sample to minimize the exposure to the laser light.

Sample preparation

The sample consists of 12–14 day-old transgenic Arabidopsis seedlings expressing the cytosolic (NES-YC3.6) or nuclear (NLS-YC3.6) localized Cameleon YC3.6. The generation of these lines was previously reported in Ref. [19] in which the full description of the targeting strategies is reported. The seeds are surface sterilized by vapor-phase sterilization and directly placed, with a toothpick, over a conical plastic holder (typically a 10 μL pipette tip) [32]. The holder is filled with half strength Murashige and Skoog medium (MS, M0222 elements including Vitamins, Duchefa, <http://www.duchefa-biochemie.nl/>) [33] supplemented with 0.1% sucrose, 2.34 mM MES with a final pH of the media to 6.0 ± 0.1 with 0.5 M KOH and 0.8% of micro agar (Duchefa). The plastic holders are then transferred to a transparent plastic box filled with sterile half strength MS solution for hydroponic culture and placed in a growth chamber under 16/8 h cycles of white light at 22 $^\circ\text{C}$. The hydroponic system allows the seedling roots to grow, following the positive gravitropism, first into the agar and subsequently directly in hydroponic solution when they reach the bottom hole of the holder. Once the root comes out the hole of the plastic holder, the specimen is transferred to the SPIM-FRET setup into the imaging chamber filled with the desired solution (for our Ca^{2+} dynamic analyses a 10 mM MES, 5 mM KCl, 10 mM CaCl_2 , pH 5.8 adjusted with TRIS-BASE solution was employed). This procedure prevents any kind of damage or major stress to the root and maintains the seedling vertical. For the analysis of spatiotemporal dynamics of the $[\text{Ca}^{2+}]$ rise, a volume of 120 μL (100X) glutamate (L-Glu) or external ATP (eATP) was directly

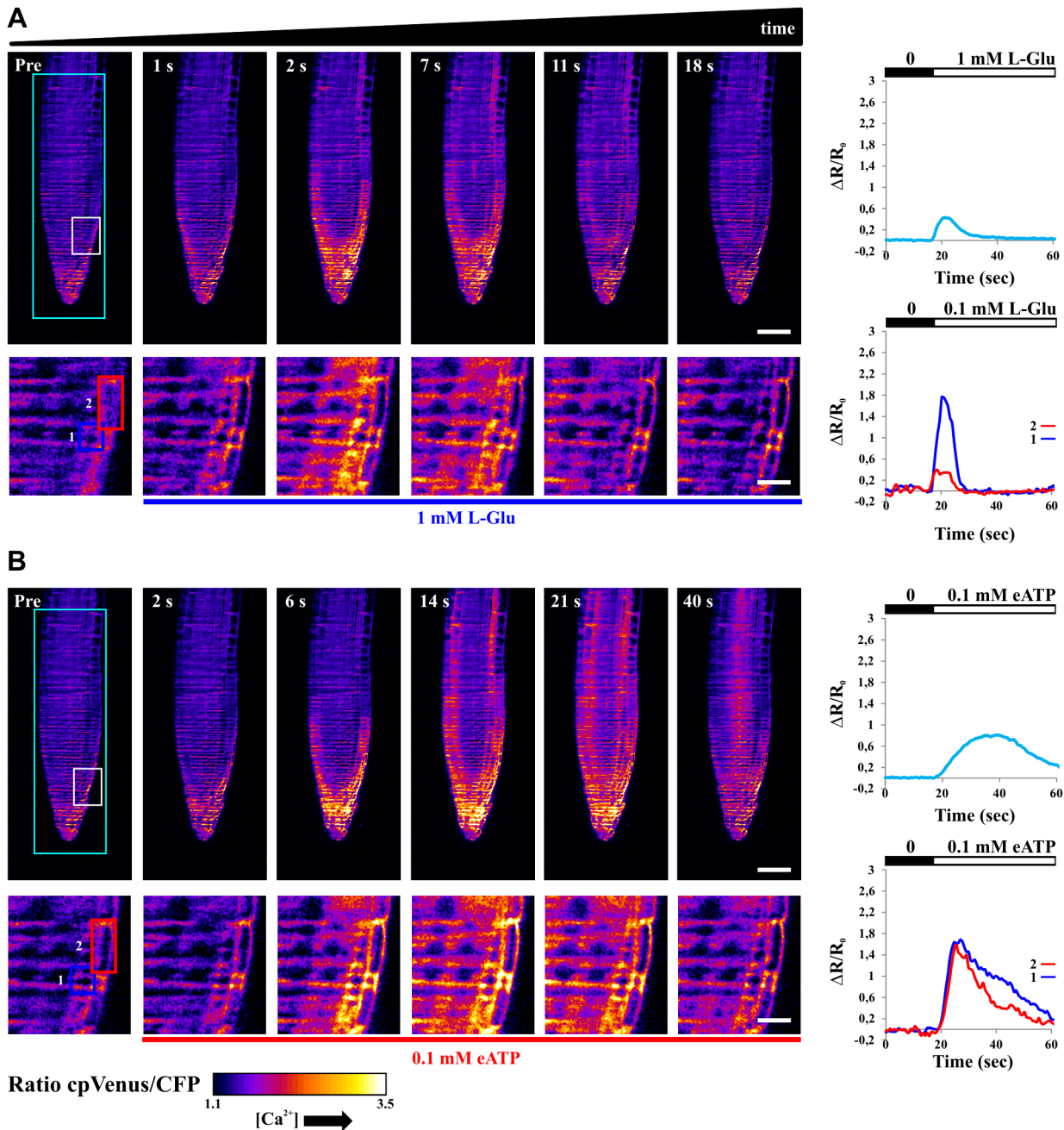


Figure 4. Single plane FRET ratio in root tip of Arabidopsis seedlings expressing the cytosolic localized Cameleon, measured at different times in the course of 1 mM L-Glu (A) and 0.1 mM eATP (B) stimuli. (A) Upper images: FRET ratio measured at different time points from the sensing (Pre) of the L-Glu stimulus. Lower images: close up (white rectangle in the top-left image) of the same selected FRET ratios. Upper graph: temporal evolution of the FRET ratio for the entire region highlighted by the cyan rectangle. Bottom graph: temporal evolution of the FRET ratios for two selected cells (blue and red rectangles in the lower images). (B) Upper images: FRET ratio measured at different time points from the sensing (Pre) of the eATP stimulus. Lower images: close up (white rectangle in the top-left image) of the same selected FRET ratios. Upper graph: temporal evolution of the FRET ratio for the entire region highlighted by the cyan rectangle. Bottom graph: temporal evolution of the FRET ratios for two selected cells (blue and red rectangles in the lower images). Scale bar is 50 μ m and 9 μ m for low and high magnifications respectively. doi:10.1371/journal.pone.0075646.g004

added to one corner of the imaging chamber (filled with 12 mL of imaging solution). The final concentration of the stimuli was 1 mM and 0.1 mM for L-Glu and eATP respectively. The stock ATP solution was diluted in a TRIS buffer (pH 5.8) in order to prevent any pH change of the imaging solution.

Imaging procedure

In the course of SPIM acquisition the root was imaged simultaneously by the 2 CCDs of the dual-sensor camera (Orca D2, Hamamatsu Photonics K.K.) and automatically translated with steps of 1 to 10 μ m to create a 3D reconstruction of a large

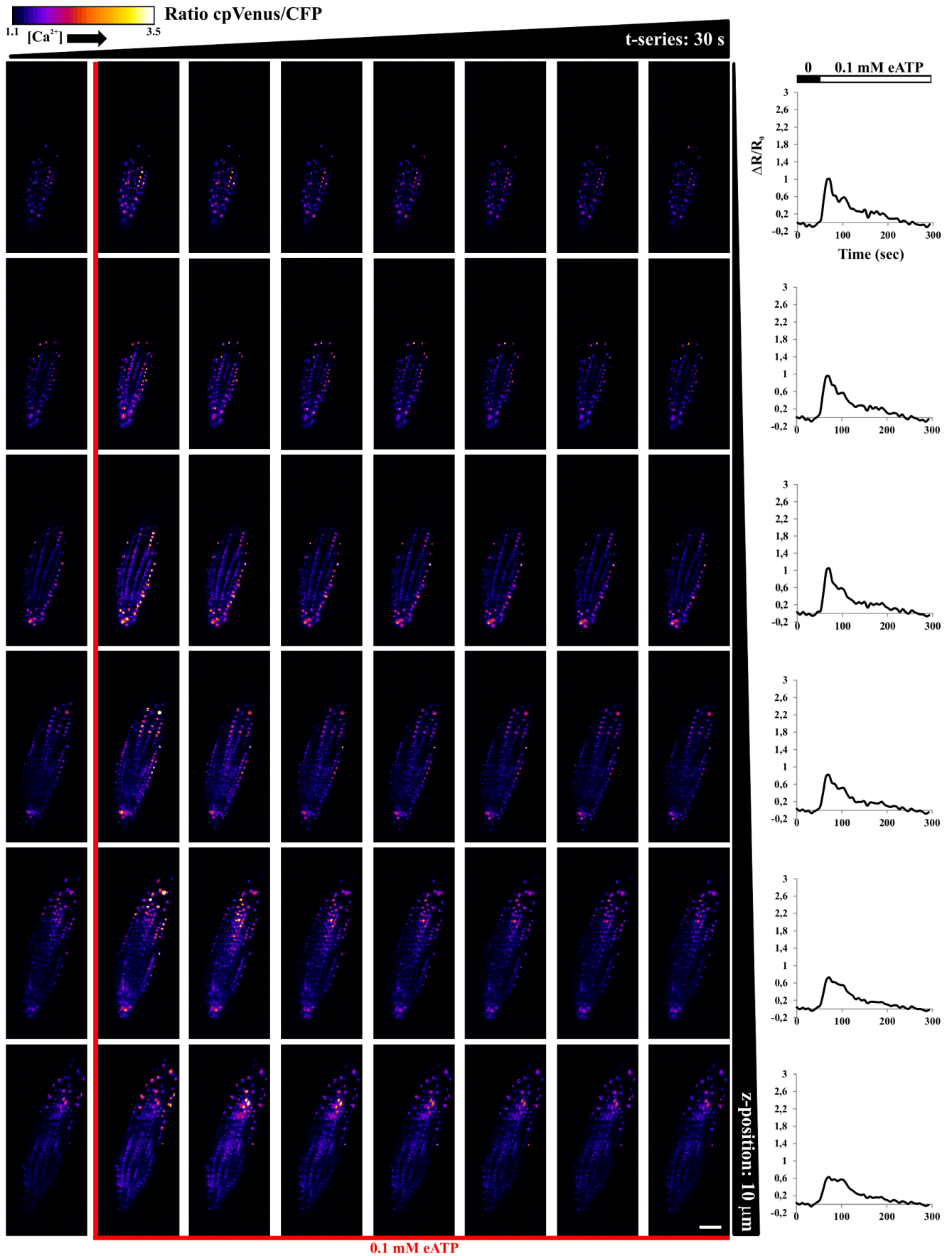


Figure 5. FRET ratio imaged in space and time, with 10 μm steps (columns) and every 30 s (rows), in root tip of *Arabidopsis* seedlings expressing the nuclear localized Cameleon, in the course of 0.1 mM eATP stimulus. Graphs on the right hand side show temporal evolution of the averaged FRET ratio for each single selected plane. Scale bar is 50 μm . doi:10.1371/journal.pone.0075646.g005

tissue volume by generating multiple image stacks. The shutter, the translation stage and the camera were controlled using Micro-Manager (www.micro-manager.org). This software enables the user to easily program the scanning of the sample over the light sheet and time-lapse acquisition parameters at the beginning of each experiment. The exposure time for each plane was typically 50–500 ms. Two different types of acquisitions were carried out: i) two-dimensional analysis, in which a single plane was imaged with continuous illumination and multiple acquisitions lasting 60–300 s; ii) three-dimensional analysis, in which several planes (typically 10–20) were acquired successively: every 5–10 s the acquisition of the entire stack was repeated. The fluorescence intensity was determined over Regions Of Interests (ROIs) corresponding to large root tip areas, single cells or nuclei. Background subtraction was performed in each channel before FRET ratio calculation by selecting a ROI outside the sample. The FRET ratio (R) was calculated and visualized using the Ratio Plus Plugin for Fiji (<http://fiji.sc/>) or NisElement (Nikon). For time course experiments the change in the FRET ratio (ΔR) was normalized to the initial value (R_0) and plotted *versus* time ($\Delta R/R_0$).

Results and Discussion

Image quality

Three different regions of the seedling root (primary root tip, lateral root primordium and root mature zone) are shown in Figure 2. The raw data corresponding to the primary root tip are presented in Figure S1. Single nuclei can be distinguished not only in the thicker mature zone, but also in developing organs such as the lateral root primordium, where cells are still clustered together (see also Movies S1, S2, S3). The achievable resolution depends on scattering and absorption properties of the sample and the image quality decreases as the optical path length increases. Therefore, the side of the sample which is closer to the camera tends to be sharper than the opposite side (see also Figure S1). However, notwithstanding the presence of strong scattering at the excitation wavelength (442 nm), these images show sub cellular details in depth over a large tissue volume (root diameter is approximately 100 μm). Further improvement of the image quality could be achieved using multi-view SPIM [34], multi-directional SPIM [31] or two-photon excitation [35]. It is worth noting that the use of water immersion objectives substantially improves the quality of the image compared to other approaches in which the sample is immersed in a cuvette and air objectives are used: image deconvolution [29] was not applied to the present data. The 3D reconstructions of the acquired root regions (Movies S1, S2, S3) show the SPIM ability to provide high resolution imaging over a large part of the specimen, a result that is difficult to reach with standard CLSM [28,36].

FRET response

One of the current and future challenges for biologists is the possibility to perform analyses of single cells laying in their natural context avoiding undesired environmental perturbation. In this view, SPIM has proved suitable for long-term visualization of *Arabidopsis* root growth in near physiological conditions during imaging [28,29]. A further step is to use this microscopy modality to monitor intracellular responses, such as stimulus-induced Ca^{2+}

mobilization, at single cell resolution and in unstressed conditions. In order to reach this goal we performed a series of experiments with *Arabidopsis* seedling expressing nuclear or cytosolic localized Cameleon YC3.6 [19].

Figure 3 shows the FRET ratio measured in the nuclei of a single plane of the primary root of *Arabidopsis* expressing the nuclear localized Cameleon. Figure 3A presents the nuclear response after treatment with 1 mM Glutamate (L-Glu), a stimulus known to induce Ca^{2+} rises in plant cells [37]. Indeed, the treatment induces a Ca^{2+} peak in the cells of the entire root tip. This is visualized as a change in the FRET ratio, which corresponds to Ca^{2+} variations (the higher the ratio the higher the Ca^{2+} concentration [21]). A more detailed analysis reveals that the response to L-Glu was primarily sensed by the nuclei of the lateral root cap cells, followed by the response of the nuclei located in the upper part of the root tip (see Movie S4). Additionally distinct individual responses of single cells can be observed: the Ca^{2+} peaks measured on 6 distinct nuclei (highlighted in green in Figure 3A) show differences both in amplitudes and temporal delay (lower panel, left). Averaging the curves over the six nuclei leads to a broader time curve (Figure 3A, lower panel, center) and when the average is calculated on the entire plane we can observe a considerably longer response (Figure 3A, lower panel, right), which mimics the response achievable at lower resolution [38].

Few minutes after the recovery from the treatment with L-Glu, the same root was treated with a second stimulus consisting in external ATP (0.1 mM eATP), which has also been reported to induce intracellular Ca^{2+} rise in plant cells [19,20,24]. As for L-Glu, the cells of the lateral root cap primarily sensed the eATP followed by the nuclei located in the transition and elongation zones (Movie S5). It is worth noting that the images were acquired with SPIM in the same plane of the sample in the course of the two stimuli and the very same nuclei are visualized in Figure 3A, B. In particular, for the 6 nuclei (labeled in green in Figure 3A, B) the L-Glu stimulus produces single and narrow peaks, whereas eATP induces a more sustained Ca^{2+} transient, pointing out to the existence of different mechanisms responsible for the generation of the observed triggered Ca^{2+} dynamics.

Each experiment (injection of L-Glu first and eATP later) was repeated $n = 6$ times. The reproducibility of the responses is shown in Figure S2A, B. We observed similar responses in all experiments whereas in $n = 3$ control experiments (injection of the solution without any Ca^{2+} mobilizing agent) the FRET changes were below the camera noise.

The comparison of the two stimuli demonstrates that SPIM offers sufficient spatial and temporal resolution to appreciate single cell responses, while monitoring large sample sizes. In Figure 3, nuclei appear as isolated and well-defined fluorescent spots, facilitating the analyses of single cells. In order to fully validate the SPIM approach, we repeated the experiments in root tip cells of *Arabidopsis* seedlings expressing the cytosolic localized Cameleon [19]. Figure 4A, B show the response of a root tip to L-Glu and eATP respectively, again acquired on the same plane with SPIM. In accordance to what observed with nuclei, the response to the two stimuli was primarily sensed by lateral root cap cells, followed by the response of cells present in deeper tissue, with a spread of $[\text{Ca}^{2+}]$ rises towards the cells of the transition and elongation zones (see Movie S6, S7 where Ca^{2+} propagation/percolation is observable). The comparison of the two stimuli (L-Glu and

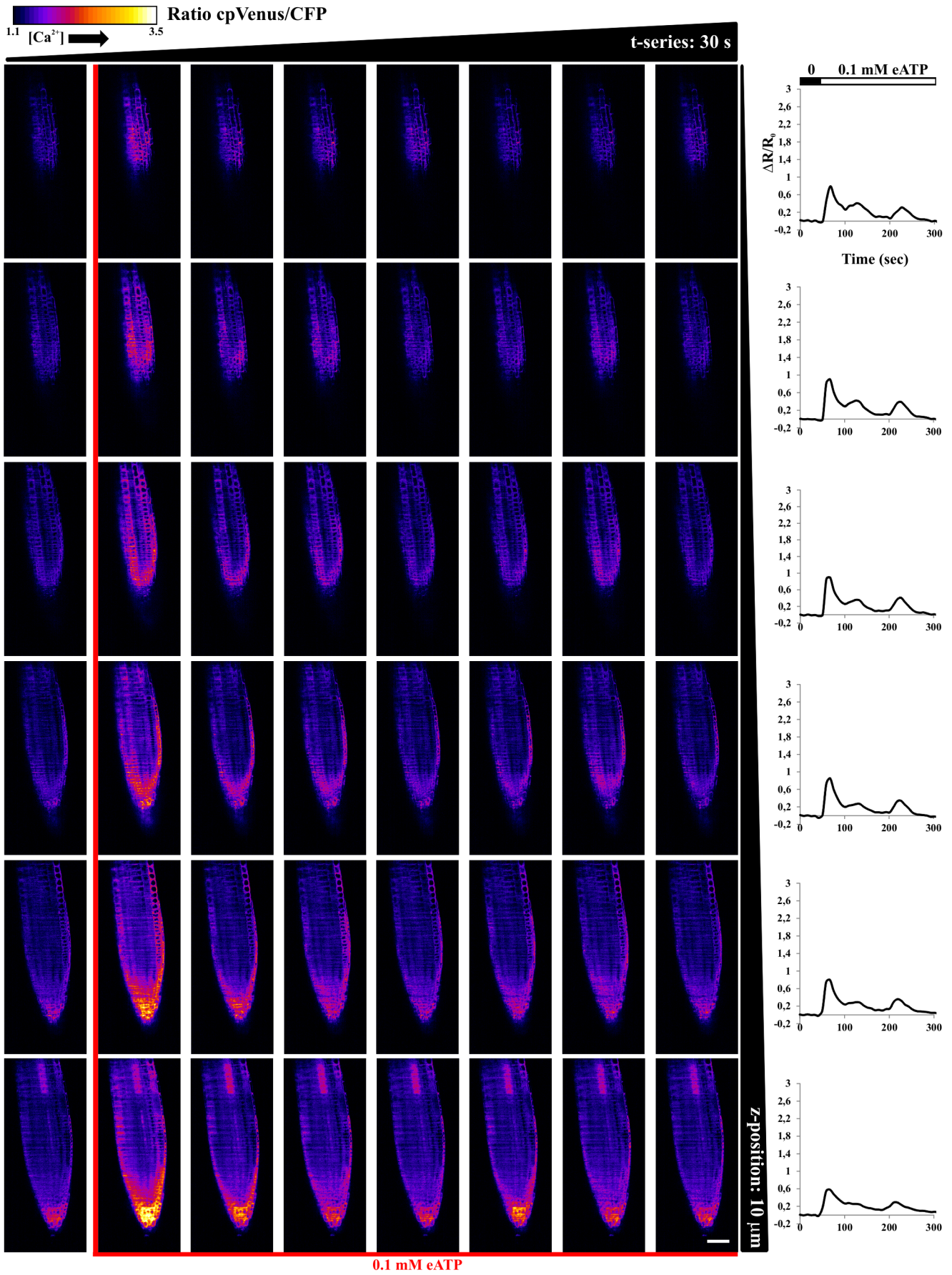


Figure 6. FRET ratio imaged in space and time, with 10 μm steps (columns) and every 30 s (rows), in root tip of *Arabidopsis* seedlings expressing the cytosolic localized Cameleon, in the course of 0.1 mM eATP stimulus. Graphs on the right hand side report temporal evolution of the average FRET ratio for each single selected plane. Scale bar is 50 μm . doi:10.1371/journal.pone.0075646.g006

eATP), performed by plotting the average FRET responses of the entire imaged plane (cyan curve in Figure 4A, B), allows one to appreciate that L-Glu and eATP produced similar Ca^{2+} peak amplitudes with different dynamics, being eATP able to induce more sustained Ca^{2+} rises than L-Glu (see also Figure S2A, B). Double peaks are also present at longer times, as shown later. Conversely, the analysis performed in two selected lateral root cap cells (blue and red curves in Figure 4A, B) shows that they respond with very different peak amplitudes in the course of L-Glu administration. Instead, their response is similar with eATP. These data, in agreement with previous reports [38,39], indicate that the kinetic analysis of an averaged response does not necessarily reflect the response of a single cell.

Although understanding the mechanisms underlying the observed differences in terms of nuclear and cytosolic Ca^{2+} dynamics in response to the two stimuli, is beyond the aim of the present work, the different responses demonstrate that the use of SPIM with plants expressing a genetically encoded Ca^{2+} probe, offers an adequate resolution to perform single cell analysis over a complex organ. Moreover, the fast acquisition rate (typically 2–10 Hz for a single plane), enables one to obtain an easy visualization of Ca^{2+} signal percolation in plants (see also Movies S4, S5, S6, S7) [39]. In order to demonstrate the SPIM ability to perform 3D analysis we treated primary root tips of *Arabidopsis* seedlings with 0.1 mM eATP, acquiring adjacent image planes (typically 10 planes, with 5–10 μm steps, every 5–8 s), in the course of the stimulus. Figure 5 and 6 show the FRET ratio imaged at different times and depths (Z-position). Note that only a subset of the acquired planes and time points are presented. The temporal FRET responses, averaged on each plane, allows one to observe that the entire organ responds to eATP, with differences among planes. In particular, every plane shows different responses in terms of peak amplitudes and dynamics (see graphs in the right hand side of Figure 5, 6). The cytosolic Ca^{2+} dynamics present several oscillations, whereas the responses of the nuclei show less resolved peaks, as we previously observed with wide-field microscopy [20]. A 3D reconstruction of the sample over time is possible, as shown in Movies S7, S8. In this case, the entire root tip can be visualized, allowing one to observe fine details of the nuclei and the cytosols. At the same time, it is possible to observe the systemic root tip response. Similar results could not be reached by means of wide-field microscopy (Figure S3A), which can be used to visualize large plant volumes, due to the lack of optical sectioning and single cell resolution.

Comparison with CLSM

Single cell visualization of intracellular Ca^{2+} dynamics in a root tip layer has been reported by some authors [24,40] along with a recently published detailed protocol to image Cameleon with CLSM has been recently published [41]. The results presented in Figure 3, 4 show that SPIM is indeed an alternative approach to CLSM, in terms of imaging quality. SPIM has lower spatial resolution than CLSM (Figure S3), but it is still able to offer subcellular detail in a large tissue volume. SPIM seems to have a higher temporal resolution than standard CLSM since it allows one to study Ca^{2+} dynamics in multiple planes in a time window compatible with relatively fast (few seconds) biological events. In particular, when 3D reconstructions are taken into consideration the photobleaching caused by the selective illumination of single planes has been reported to be orders of magnitude lower than the

one caused by CLSM [27,42]. A further advantage is the simplicity of the setup and its low cost (for an estimate of the cost see Ref. [30]).

Although a quantitative comparison of the techniques strongly depends on the actual CLSM microscope employed, a parallel series of experiments were carried out with CLSM and SPIM (Figure S3B, C). The experiments consisted in the injection of 0.1 mM of eATP to induce an increase and oscillation in Ca^{2+} , lasting up to 5 min (Figure S3A). In SPIM, some horizontal lines appeared in the images, caused by the presence of shadows within the light sheet. These lines can however be removed by hardware [31]. The contrast is slightly lower with SPIM, mainly because of the noise of the camera (note that in Figure S3A background subtraction was not applied). Nevertheless, we observed a stronger response with SPIM ($+35 \pm 10\%$, $n = 3$), thanks to the higher dynamic range of the camera. Finally a larger region of the sample could be imaged with SPIM.

Hence, SPIM combines the advantages of different microscopy approaches in a single technique. As a matter of fact, single cell resolution, typical of CLSM techniques is coupled with the ability to observe systemic root responses, characteristic of wide field microscopy.

Conclusions

The above presented data indicate that the developed SPIM-FRET method is ideally suited to monitor Ca^{2+} signaling *in vivo*, at high resolution, with negligible photo-bleaching and in depth over a large tissue volume. The instrument is relatively simple and cost effective. Such technology could lead to many different experiments that combine developmental programs with environmental stimuli. Imaging of Ca^{2+} using SPIM-FRET is not limited to plant biology but can be used for 3D mapping of Ca^{2+} dynamics in a variety of semi-transparent biological samples including embryos such as zebrafish (*Danio rerio*) and *Drosophila melanogaster*.

Supporting Information

Figure S1 Sagittal (A–C) and two transverse sections (D–I) of the specimen (*Arabidopsis* expressing the nuclear localized Cameleon) for CFP signal, cpVenus and FRET ratio. The sagittal sections are acquired within approximately one third of the sample thickness. The transverse sections are obtained scanning the entire sample within the light sheet. Scale bar is 50 μm .

(TIF)

Figure S2 Statistical analysis of the response amplitude and duration, in root tip of *Arabidopsis* seedlings expressing the nuclear or cytosolic localized Cameleon, for 0.1 mM eATP and 1 mM L-Glu stimuli. (A) Mean value of the FRET ratio changes measured on the peak of the response ($\Delta R_{\text{max}}/R_0$). (B) Mean value of the FRET ratio changes measured 40 s after the stimulus ($\Delta R_{40}/R_0$). The eATP response is still active at long times while the L-Glu response is depleted. Values are means \pm SE ($n = 6$). p-values were calculated by Student's t test.

(TIF)

Figure S3 Comparison of different microscopy modalities for measuring eATP-induced Ca^{2+} dynamics in root tip of *Arabidopsis* seedlings expressing the cytosolic localized Cameleon. Selected FRET ratios images of the root tip at different time points

from the sensing (Pre) of the eATP stimulus acquired with: (A) Wide-field microscopy with a 20× detection objective as described in Ref. [20]; (B) CLSM analysis. The images were acquired with a 63× water immersion objective as described in Ref. [41]; (C) SPIM microscopy. The images were acquired with a 20× objective as described in Material and methods. Scale bar is 50 μm. Background subtraction was not applied to these experiments.
(TIF)

Movie S1 Three-dimensional (3D) reconstruction of the primary root tip of *Arabidopsis thaliana* (CFP fluorescence signal) expressing the nuclear localized Cameleon.
(MP4)

Movie S2 Three-dimensional (3D) reconstruction of a lateral root primordium of *Arabidopsis thaliana* (CFP fluorescence signal) expressing the nuclear localized Cameleon.
(MP4)

Movie S3 Three-dimensional (3D) reconstruction of the root mature zone of *Arabidopsis thaliana* (CFP fluorescence signal) expressing the nuclear localized Cameleon.
(MP4)

Movie S4 Time series of nuclear FRET ratio images of an Arabidopsis seedling root tip expressing the nuclear localized Cameleon challenged with 1 mM L-Glu. The movie plays 4 times at real-time.
(AVI)

Movie S5 Time series of nuclear FRET ratio images of an Arabidopsis seedling root tip expressing the nuclear localized Cameleon challenged with 0.1 mM eATP. The movie plays 4 times at real-time.
(AVI)

Movie S6 Time series of cytosolic FRET ratio images of an Arabidopsis seedling root tip expressing the cytosolic localized

Cameleon challenged with 1 mM L-Glu. The movie plays 4 times at real-time.
(AVI)

Movie S7 Time series of cytosolic FRET ratio images of an Arabidopsis seedling root tip expressing the cytosolic localized Cameleon challenged with 0.1 mM eATP. The movie plays 4 times at real-time.
(AVI)

Movie S8 Time lapse 3D reconstruction of nuclear FRET ratio of an Arabidopsis seedling root tip expressing the nuclear localized Cameleon challenged with 0.1 mM eATP. The movie plays 20 times at real-time.
(AVI)

Movie S9 Time lapse 3D reconstruction of cytosolic FRET ratio of an Arabidopsis seedling root tip expressing the cytosolic localized Cameleon challenged with 0.1 mM eATP. The movie plays 20 times at real-time.
(AVI)

Acknowledgments

We thank Dr. Karin Schumacher at University of Heidelberg for providing us the UBQ10-NES-YC3.6 and UBQ10-NLS-YC3.6 Arabidopsis plants. We thank Peter G. Pitrone and Jan Huisken at MPI Dresden for their suggestions on the imaging chamber construction and Mauro Bombonati at Hamamatsu Photonics for his help with the camera settings. We thank Smrutisanjita Behera at University of Münster for sharing previously unpublished data now reported in Figure S3B.

Author Contributions

Conceived and designed the experiments: A. Costa AB. Performed the experiments: A. Costa A. Candeo AB. Analyzed the data: A. Costa LF GV AB. Contributed reagents/materials/analysis tools: A. Costa A. Candeo LF GV AB. Wrote the paper: A. Costa AB.

References

- Dodd AN, Kudla J, Sanders D (2010) The language of calcium signaling. *Annu Rev Plant Biol* 61: 593–620.
- Kudla J, Batistic O, Hashimoto K (2010) Calcium signals: the lead currency of plant information processing. *Plant Cell* 22: 541–563.
- Allen GJ, Chu SP, Schumacher K, Shimazaki CT, Vafeados D, et al. (2000) Alteration of stimulus-specific guard cell calcium oscillations and stomatal closing in Arabidopsis *det3* mutant. *Science* 289: 2338–2342.
- Allen GJ, Chu SP, Harrington CL, Schumacher K, Hoffmann T, et al. (2001) A defined range of guard cell calcium oscillation parameters encodes stomatal movements. *Nature* 411: 1053–1057.
- Young JJ, Mehta S, Israelsson M, Godoski J, Grill E, et al. (2006) CO₂ signaling in guard cells: calcium sensitivity response modulation, a Ca²⁺-independent phase, and CO₂ insensitivity of the *gca2* mutant. *Proc Natl Acad Sci U S A* 2006 103: 7506–7511.
- McAinsh MR, Pittman JK (2009) Shaping the calcium signature. *New Phytol* 181: 275–294.
- Mazars C, Brière C, Bourque S, Thuleau P (2011) Nuclear calcium signaling: An emerging topic in plants. *Biochimie* 93: 2068–2074.
- Love J, Dodd AN, Webb AAR (2004) Circadian and diurnal calcium oscillations encode photoperiodic information in Arabidopsis. *Plant Cell* 16: 956–966.
- Short EF, North KA, Roberts MR, Hetherington AM, Shirras AD, et al. (2012) A stress-specific calcium signature regulating an ozone-responsive gene expression network in Arabidopsis. *Plant J* 71: 948–961.
- Kosuta S, Hazledine S, Sun J, Miwa H, Morris RJ, et al. (2008) Differential and chaotic calcium signatures in the symbiosis signaling pathway of legumes. *Proc Natl Acad Sci U S A* 105: 9823–9828.
- Whalley HJ, Sargeant AW, Steele JF, Lacoere T, Lamb R, et al. (2011) Transcriptomic analysis reveals calcium regulation of specific promoter motifs in Arabidopsis. *Plant Cell* 23: 4079–4095.
- Whalley HJ, Knight MR (2013) Calcium signatures are decoded by plants to give specific gene responses. *New Phytol* 197: 690–693.
- Knight MR, Campbell AK, Smith SM, Trethewey AJ (1991) Transgenic plant aequorin reports the effects of touch and cold-shock and elicitors on cytoplasmic calcium. *Nature* 352: 524–526.
- Allen GJ, Kwak JM, Chu SP, Llopis J, Tsien RY, et al. (1999) Cameleon calcium indicator reports cytoplasmic calcium dynamics in Arabidopsis guard cells. *Plant J* 19: 735–747.
- Costa A, Drago I, Behera S, Zottini M, Pizzo P, et al. (2010) H₂O₂ in plant peroxisomes: an *in vivo* analysis uncovers a Ca²⁺-dependent scavenging system. *Plant J* 62: 760–772.
- Rincón-Zachary M, Teaster ND, Sparks JA, Valster AH, Motes CM, et al. (2010) Fluorescence resonance energy transfer-sensitized emission of yellow cameleon 3.60 reveals root zone-specific calcium signatures in Arabidopsis in response to aluminum and other trivalent cations. *Plant Physiol* 152: 1442–1458.
- Sieberer BJ, Chabaud M, Timmers AC, Monin A, Fournier J, et al. (2009) A nuclear-targeted cameleon demonstrates intranuclear Ca²⁺ spiking in *Medicago truncatula* root hairs in response to rhizobial nodulation factors. *Plant Physiol* 151: 1197–1206.
- Swanson SJ, Choi WG, Chanoca A, Gilroy S (2011) *In vivo* Imaging of Ca²⁺, pH, and Reactive Oxygen Species Using Fluorescent Probes in Plants. *Annu Rev Plant Biol* 62: 273–297.
- Krebs M, Held K, Binder A, Hashimoto K, Den Herder G, et al. (2012) FRET-based genetically encoded sensors allow high-resolution live cell imaging of Ca²⁺ dynamics. *Plant J* 69: 181–192.
- Loro G, Pozzan T, Lo Schiavo F, Zottini M, Costa A (2012) Targeting of Cameleons to various subcellular compartments reveals a strict cytoplasmic/mitochondrial Ca²⁺ handling relationship in plant cells. *Plant J* 71: 1–13.
- Palmer AE, Tsien RY (2006) Measuring calcium signaling using genetically targetable fluorescent indicators. *Nat Protoc* 1: 1057–1065.
- Nagai T, Yamada S, Tominaga T, Ichikawa M, Miyawaki A (2004) Expanded dynamic range of fluorescent indicators for Ca²⁺ by circularly permuted yellow fluorescent proteins. *Proc Natl Acad Sci USA* 101: 10554–10559.
- Loro G, Ruberti C, Zottini M, Costa A (2013) The D3cpv Cameleon reports Ca²⁺ dynamics in plant mitochondria with similar kinetics of the YC3.6 Cameleon, but with a lower sensitivity. *J Microsc* 249: 8–12.
- Tanaka K, Swanson SJ, Gilroy S, Stacey G (2010) Extracellular nucleotides elicit cytosolic free calcium oscillations in Arabidopsis. *Plant Physiol* 154: 705–719.

25. Monshausen GB, Messerli MA, Gilroy S (2008) Imaging of the Yellow Cameleon 3.6 indicator reveals that elevations in cytosolic Ca^{2+} follow oscillating increases in growth in root hairs of *Arabidopsis*. *Plant Physiol* 147: 1690–1698.
26. Band LR, Wells DM, Larrieu A, Sun J, Middleton AM, et al. (2012) Root gravitropism is regulated by a transient lateral auxin gradient controlled by a tipping-point mechanism. *Proc Natl Acad Sci U S A* 109: 4668–4673.
27. Huisken J, Swoger J, del Bene F, Wittbrodt J, Stelzer EH (2004) Optical Sectioning Deep Inside Live Embryos by Selective Plane Illumination Microscopy. *Science* 305: 1007–1009.
28. Maizel A, von Wangenheim D, Federici F, Haseloff J, Stelzer EH (2011) High-resolution live imaging of plant growth in near physiological bright conditions using light sheet fluorescence microscopy. *Plant J* 68: 377–385.
29. Sena G, Frenz Z, Birnbaum KD, Leibler S (2011). Quantitation of Cellular Dynamics in Growing *Arabidopsis* Roots with Light Sheet Microscopy. *PLoS ONE* 6(6): e21303.
30. Pitrone PG, Schindelin J, Stuyvenberg L, Preibisch SW, Weber M, et al. (2013) OpenSPIM: an open access light sheet microscopy platform. *Nat Methods* 10: 598–599.
31. Huisken J, Stainier DYR (2007) Even fluorescence excitation by multidirectional selective plane illumination microscopy (mSPIM). *Opt Letts* 32(17): 2608–2610.
32. Grossmann G, Guo WJ, Ehrhardt DW, Frommer WB, Sit RV, et al. (2011) The RootChip: an integrated microfluidic chip for plant science. *Plant Cell* 23: 4234–4240.
33. Murashige T, Skoog F (1962) A revised medium for rapid growth and bioassays with tobacco tissue cultures. *Physiol Plant* 15: 473–497.
34. Swoger J, Verveer P, Greger K, Huisken J, Stelzer EHK (2007) Multi-view image fusion improves resolution in three-dimensional microscopy. *Opt Express* 15: 8029–8042.
35. Truong TV, Supatto W, Koos DS, Choi JM, Fraser SE (2011) Deep and fast live imaging with two-photon scanned light-sheet microscopy. *Nat Methods* 8: 757–760.
36. Ntziachristos V (2006) Fluorescence molecular imaging. *Annu Rev Biomed Eng* 8:1–33.
37. Qi Z, Stephens NR, Spalding EP (2006) Calcium entry mediated by GLR3.3, an *Arabidopsis* glutamate receptor with a broad agonist profile. *Plant Physiol* 142: 963–71.
38. Dodd AN, Jakobsen MK, Baker AJ, Telzerow A, Hou SW, et al. (2006) Time of day modulates low-temperature Ca signals in *Arabidopsis*. *Plant J* 48: 962–973
39. Plieth C (2010) Signal percolation through plants and the shape of the calcium signature. *Plant Signal Behav* 5: 379–385.
40. Zhu X, Feng Y, Liang G, Liu N, Zhu JK (2013) Aequorin-based luminescence imaging reveals stimulus- and tissue-specific Ca^{2+} dynamics in *Arabidopsis* plants. *Mol Plant* 6: 444–455.
41. Behera S, Kudla J (2013) High-resolution imaging of cytoplasmic Ca^{2+} dynamics in *Arabidopsis* roots. *Cold Spring Harb Protoc* 1:2013(7).
42. Huisken J, Stainier DY (2009) Selective plane illumination microscopy techniques in developmental biology. *Development* 136(12): 1963–1975.